



**Entangled Chain Polymer Liquids Under Continuous Shear  
Deformation: Consequences of a Microscopically  
Anharmonic Confining Tube**

Journal:	<i>Soft Matter</i>
Manuscript ID	SM-ART-06-2018-001182.R1
Article Type:	Paper
Date Submitted by the Author:	04-Aug-2018
Complete List of Authors:	Xie, Shi-Jie; University of Illinois at Urbana-Champaign, Materials Science and Engineering Schweizer, Kenneth; University of Illinois at Urbana-Champaign,

Soft Matter, revised, August 2018

**Entangled Chain Polymer Liquids Under Continuous Shear  
Deformation: Consequences of a Microscopically Anharmonic  
Confining Tube**

Shi-Jie Xie<sup>1</sup> and Kenneth S. Schweizer<sup>1-4,\*</sup>

Departments of Materials Science<sup>1</sup>, Chemistry<sup>2</sup>, Chemical & Biomolecular Engineering<sup>3</sup>,  
and Frederick Seitz Materials Research Laboratory<sup>4</sup>, University of Illinois, 1304 West  
Green Street, Urbana, IL 61801, USA

[\\*kschweiz@illinois.edu](mailto:kschweiz@illinois.edu)

## ABSTRACT

We generalize our non-classical theory for the shear rheology of entangled flexible polymer liquids to address the consequences of a deformation-modified anharmonic tube confinement field. Numerical results for stress-strain curves, orientational relaxation time, primitive path (PP) step orientational order parameter, dynamic tube diameter and transverse entropic barrier under nonequilibrium conditions are presented as a function of dimensionless shear rate, strain and degree of entanglement. Deformation-induced changes of the tube field have essentially no effect on rheology under fast deformations conditions corresponding to Rouse Weissenberg numbers  $Wi_R > 1$  because of the dominance of PP chain stretch. However, the scaling behavior of the effective orientational relaxation time and rheological response at low deformation rates  $Wi_R < 1$  are significantly modified, with the stress overshoot coordinates predicted to become shear rate and degree of entanglement dependent. Stress-assisted transverse activated barrier hopping as a new channel of orientational relaxation is found to be potentially important when  $Wi_R < 1$ . The dynamic tube diameter and transverse entropic barrier that confines chains in a tube are rich functions of strain, shear rate and degree of entanglement. Deformation can increase or decrease the tube diameter, and non-monotonic changes with strain are possible due to competing consequences of PP orientation, chain stretch and stress. The transverse barrier is relatively high for all strains below the stress overshoot, for weaker entanglement, and for  $Wi_R > 1$ , corresponding to a dynamically stable tube. But for high enough degrees of entanglement and  $Wi_R < 1$ , although the barrier still exists it can become very low.

## I. Introduction

The construction of a molecular and force-level predictive theory of the complex nonlinear rheological behavior of entangled synthetic and biological polymer liquids remains a grand theoretical challenge [1-4]. In contrast to equilibrium dynamics for which there exists the successful reptation-tube phenomenological theory [1-3], nonlinear rheology involves large driving forces, chain deformation and other nonequilibrium effects. Thus, additional ad hoc guesses must be made about how deformation modifies entanglements, the confining tube, primitive path (PP) contour length, etc. Beginning with Doi and Edwards (DE) [1], it is typically assumed that deformation does not modify the tube diameter and stretched chains can rapidly retract along the PP in an unentangled Rouse manner [1,3,5,6]. Recent neutron scattering experiments [7] and simulations [8] have challenged the free Rouse retraction hypothesis.

A fundamental causality question [4,9] is what is the nature of the microscopic *inter-polymer force* created by a macroscopically-applied deformation that induces chain stretching in topologically entangled polymers. Wang and coworkers have proposed the new idea of a *deformation-induced* “grip force” of interchain entanglement origin as the microscopic source of affine stretching [4,9-11]. The ability of a polymer to retract along the PP is argued to be temporally delayed (effectively there is an entropic barrier) until the elastic retraction force built by stretching exceeds the grip force, a condition called force imbalance or “loss of grip”. It was argued [4,9,10] this force imbalance condition directly determines the shear-rate-dependence of the stress overshoot. The idea that the entanglement network, and hence the tube, is “mechanically fragile” and can “yield” at the microscopic level beyond a modest threshold deformation has also been advanced by

Wang et al. [4,9-11] in an attempt to understand puzzling observations under nonlinear step strain, continuous startup deformation, and stress-controlled creep.

Very recently we constructed a new theory [12,13] for the shear rheology of entangled chain liquids based on the simplifying assumption that the tube confinement field is unchanged during continuous deformation. Five new physical features were introduced [12,13]: (i) an interchain grip force that generates chain stretch, (ii) a force imbalance condition for the termination of an affine stretch deformation, (iii) a delayed chain retraction process which *after* loss of grip is accelerated compared to the bare Rouse time  $\tau_R$  when  $Wi_R \equiv \dot{\gamma}\tau_{R,0} > 1$ , (iv) a distribution of tube diameters, (v) a convective constraint release (CCR) process that emerges only after the PP contour length begins to decrease. Quantitative predictions were made for the stress-strain curve, shear rate dependence of the stress overshoot and undershoot features,  $S_{xy}$ , PP contour length dynamics, and nonequilibrium steady state properties spanning the slow and fast deformation regimes. For slow deformations there is little or no chain stretch and our results are qualitatively the same as prior tube models [1,5,6]. However, under fast deformation conditions, we made multiple qualitatively new predictions for all rheological and dynamic properties that are not contained in existing models, all of which are in good agreement with experiment [4,11,14,15] and simulation [16-18].

The fundamental open question remains of whether the tube confinement field is truly deformation invariant, and if not what are the consequences? This is a difficult nonequilibrium dynamics question which can impact rheology, chain stretch dynamics and orientational relaxation. Purely (not involving forces) phenomenological tube models

[1-3,5,6] do not microscopically construct the transverse tube confinement field, but rather assume harmonic confinement and an effectively unbreakable tube.

The above issue has been treated in great detail by Sussman and Schweizer (SS) [19-21] for entangled rod solutions using the nonlinear Langevin equation (NLE) approach originally formulated for glassy dynamics and transient cage localization [22,23]. The full anharmonic (non-Gaussian) tube confinement potential in equilibrium has been constructed and successfully confronted with experiments on entangled F-actin solutions [21]. A *finite* maximum tube confinement force is predicted, resulting in the possibility of huge tube swelling or even complete destruction of transverse confinement under strong deformation conditions [20]. Novel rheological consequences of this aspect have been predicted for startup continuous shear [19] and nonlinear step strain relaxation [20]. Recent active microrheology experiments on F-actin solutions [24-26] have been interpreted as providing support for the SS ideas of massive tube softening, deformation-induced accelerated reptation, and a competing relaxation channel associated with transverse activated entropic barrier hopping. Sussman and Schweizer tentatively extended [27-29] the rod theory to flexible chains at the PP level, and showed that in equilibrium, the predicted transverse confinement potential is accurate compared to simulation [27]. For purely oriented chains, the theory predicts that deformation-induced orientation leads to tube expansion [28,29]. In contrast, if chains affinely stretch, the tube is predicted to be compressed [29].

The goal of the present article is to generalize our theory for the shear rheology of entangled chain liquids [12,13] to include deformation-induced changes of the tube confinement field and investigate its rheological consequences. We also study for the first

time several dynamic structural quantities under strongly nonequilibrium conditions. Section II recalls relevant elements of the SS approach for the anharmonic tube confinement field. Section III briefly reviews our recent rheology theory [12,13] and formulates the consequences of deformation-induced changes of the tube field on orientational relaxation. Section IV presents new predictions for how deformation-induced changes of the tube modify the full stress-strain response, including the stress overshoot, tube diameter, PP step orientational order parameter and other properties. Section V studies how the transverse entropic barrier evolves with strain, shear rate and degree of entanglement. The article concludes in Section VI with a discussion. Background technical details of the theory and additional calculations are presented in the Supplementary Information (SI).

## II. Theory of the Anharmonic Tube Confinement Field

### A. Overview

This section reviews, without derivation or detailed explanations which can all be found elsewhere [27-29], the construction of the full tube confinement potential based on modeling a polymer chain as a connected set of dynamically uncrossable, infinitely thin, self-consistently-determined rigid PP steps which translate but do not rotate (see Fig.1). There are *no* interchain equilibrium correlations in such a model based on objects with zero space filling volume. The tube confinement potential is constructed at the force level based on a locally “disconnected-PP” (d-PP) simplification. In general, the d-PP step has a stretch-dependent length  $L_e \equiv \lambda \cdot \kappa b \sqrt{N_e}$ , where  $\lambda$  is the stretch ratio,  $b$  is the statistical segment length, and  $\kappa$  is a numerical constant that captures missing monomer degrees of freedom [27]. The degree of nematic orientational order at the PP step level is

defined as  $S$ . Predictions of the SS approach in equilibrium quantitatively agree with simulations of entangled chain melts for the PP step probability distribution function when  $\kappa = 2.5$  [27]. Further details can be found in ref. [27-29]. Here we summarize only the essential foundational aspects relevant to our new work.

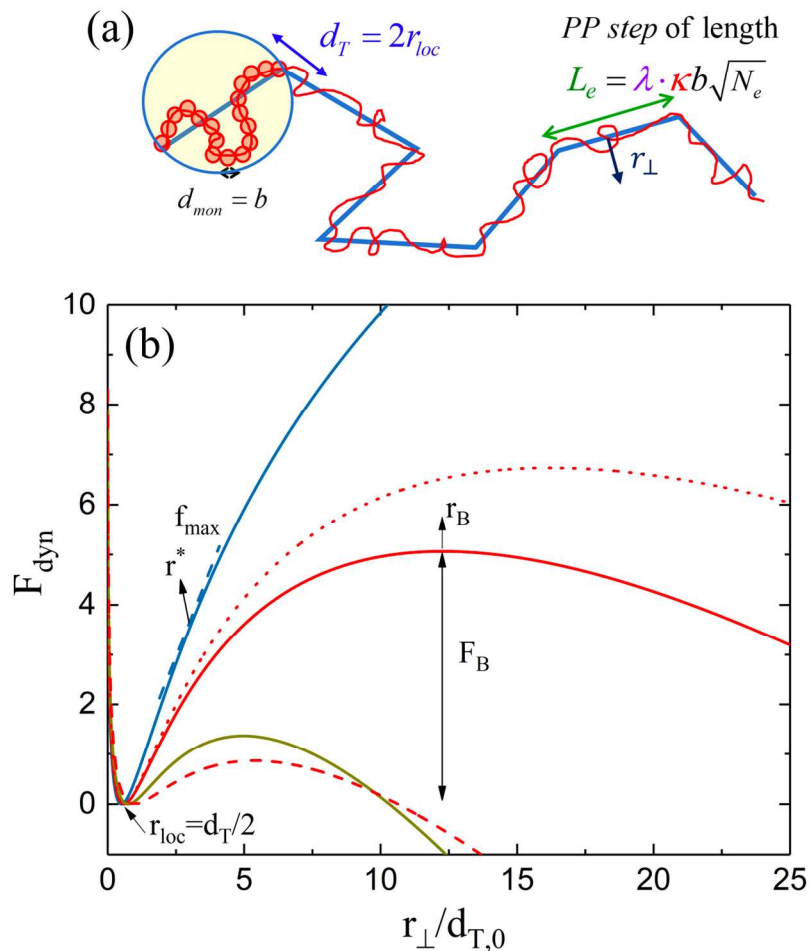


**Figure 1** (a) Schematic diagram of the primitive path (PP) chain mapping. See text for details. (b) Dynamic tube confinement potential (units of  $k_B T$ ) vs dimensionless transverse displacement of a PP step in units of the equilibrium tube diameter. From top to bottom the solid curves correspond to  $S = 0$ ,  $\lambda = 1$  and  $\sigma/G_e = 0, 1, 2$ , the dashed

curve corresponds to  $\sigma/G_e = 1$ ,  $S = 0.5$ ,  $\lambda = 1$ , and the dotted curve corresponds to  $\sigma/G_e = 1$ ,  $S = 0.5$ ,  $\lambda = 1.1$ . On the  $\sigma/G_e = 0$ ,  $S = 0$ ,  $\lambda = 1$  curve, the transverse localization length (half the tube diameter  $r_{loc} = d_T/2$ ), and the location of maximum restoring force ( $f_{max}$ ),  $r^*$ , are labeled. On the  $S = 0$ ,  $\lambda = 1$  and  $\sigma/G_e = 1$  curve the location and magnitude of the transverse barrier,  $r_B$  and  $F_B$ , respectively, are indicated.

The gradient of the anharmonic tube confinement potential, or “dynamic free energy”, describes the force on a tagged PP step due to the surrounding polymer liquid (Fig.1). Its minimum is the most probable transverse localization length which can be directly computed in a *fully self-consistent* manner based on a harmonic or Gaussian treatment of transverse displacements. This analysis has been performed for isotropic equilibrium liquids, and also liquids where the PP step length is stretched and/or oriented in a prescribed manner. Sections IIB and IIC summarize results at this level of the theory. The presence of a macroscopic nonzero stress implies PP steps also experience an additional microscopic force as discussed in section IID.

### B. Basics of Transverse Confinement Potential for Isotropic Fluids

At the Gaussian (2<sup>nd</sup> moment) level per a harmonic tube field, the self-consistent equation for the tube diameter (twice the dynamic transverse localization length),  $d_T = 2r_{loc}$ , for the general case where PP steps can be deformed or oriented is [29],

$$\frac{d_{T,0}}{P} = \frac{16\sqrt{2}\pi^2}{\kappa F \left( \frac{2\kappa\lambda}{d_T/d_{T,0}} \right) G(S)\lambda^3} \quad (1)$$

Here,  $d_{T,0}$  is the equilibrium tube diameter,  $p$  the packing length [30],  $F(x)$  carries dynamical information about the confining entanglement forces, and  $G$  quantifies the effect of PP step orientational order [28,29]. For isotropic equilibrium liquids, the theory predicts [27]  $d_{T,0} \approx 8.2p$  for  $\kappa = 2.5$ , while PP simulations [31] find  $d_{T,0} \approx 12.2p$ .

The NLE approach [22,23] goes beyond the Gaussian analysis to construct the full anharmonic tube-confinement potential which enters a nonlinear stochastic equation of motion for the transverse center-of-mass (CM) displacement ( $r_{\perp}$ ) of a PP step [27-29]

$$-\xi_s \frac{dr_{\perp}}{dt} - \frac{\partial}{\partial r_{\perp}} F_{dyn}(r_{\perp}) + \delta f_s = 0 \quad (2)$$

Here,  $\xi_s$  is a short-time friction constant (unimportant here),  $\delta f_s$  is the corresponding white-noise random force, and  $F_{dyn}(r_{\perp})$  is the "dynamic free energy" or tube confinement potential that captures entanglement constraints (*dynamic* uncrossability). The latter follows from integrating the displacement-dependent transverse force [27-29],

$$f(r_{\perp}) = \frac{2}{r_{\perp}} - \frac{2}{r_{\perp} F\left(\frac{2\kappa\lambda}{d_T/d_{T,0}}\right)} F\left(\frac{\kappa\lambda}{r_{\perp}/d_{T,0}}\right) \quad (3)$$

The Gaussian-theory result for the tube diameter corresponds to the minimum of the tube field and satisfies  $f(r_{\perp} \equiv d_T/2) = 0$ . Under equilibrium conditions the transverse barrier is *infinite* but the maximum restoring force (see Fig.1(b)) is finite,  $f_{\max} \approx 1.6 k_B T / d_{T,0}$  [27-29]. The latter is in contrast to phenomenological ansatzes of an unbreakable tube.

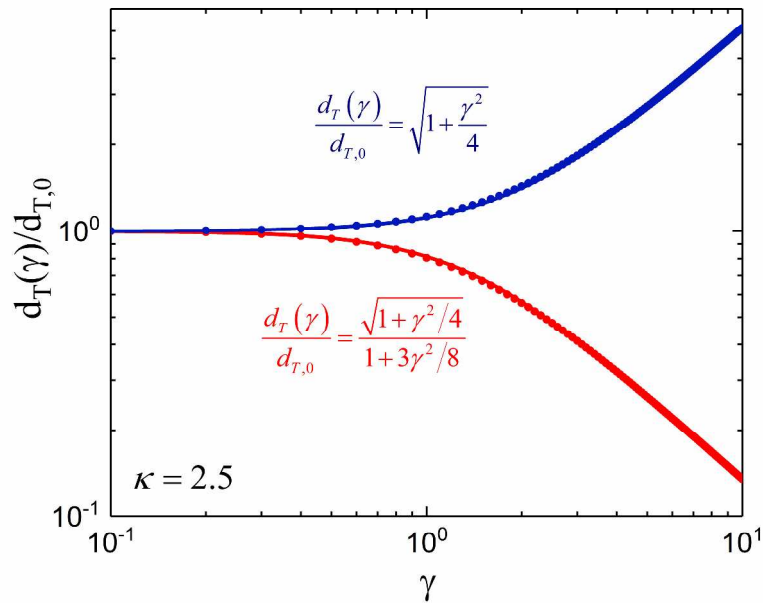


**Figure 2** Log-log plot of the tube diameter (normalized by its equilibrium value) of an entangled liquid subjected to a globally affine shear deformation as a function of shear strain. The upper results correspond to no PP stretching (only orientation), and the lower results correspond to an affinely stretched primitive path. The solid curves through the numerically-determined points are the analytic functions of Eq. (4) and Eq. (5).

### C. Effect of Affine-like Orientation and/or Chain Stretch

To explore the effect of chain orientation and stretching on the tube diameter one can insert into the dynamical theory information about PP step stretching and/or orientation, and then again solve the self-consistency equation Eq.(1). Results are shown in Fig.2 for a globally affine shear deformation [29] when  $\lambda=1$  (no stretching) and for  $\lambda \neq 1$ . Tube diameter changes can be expressed as a function of the orientational and PP stretch variables, or as a function of affine strain,  $\gamma$ . For  $\lambda=1$ , the tube diameter

increases with strain since deformation induces orientational order which reduces the consequences of dynamic intermolecular uncrossability constraints. The result is [28,29]:

$$\frac{d_T(\gamma)}{d_{T,0}} \approx \sqrt{1 + \frac{\gamma^2}{4}} \approx \frac{1}{\sqrt{1-S}} \quad (4)$$

If the PP is affinely stretched then  $\lambda = \sqrt{1 + \gamma^2/3}$ , and one has both PP orientation and a longer step length. Numerical results are well approximated by [29]:

$$\frac{d_T(\gamma)}{d_{T,0}} \approx \frac{\sqrt{1 + \gamma^2/4}}{1 + 3\gamma^2/8} \quad (5)$$

The numerator reflects orientation-driven tube swelling, while the denominator captures tube compression due to stretching. More generally, the theory predicts nontrivial coupling of PP orientation and stretching on the dynamic transverse localization length.

Changes of the tube diameter impact all other features of the dynamic free energy in the same direction. For example, pure PP orientation reduces  $f_{\max}$  thereby “softening” the tube field, while affine stretching plus orientation “hardens” the tube corresponding to a larger  $f_{\max}$ . But in all cases the transverse barrier is infinite in the “dynamic local equilibrium” framework of NLE theory and hence polymers are laterally confined.

#### **D. Direct Effect of Applied Stress and Microscopic Yielding Concept**

In a bulk rheology experiment, there are macroscopic forces per unit area applied at a boundary which must be transmitted as microscopic forces on polymer molecules. The latter should enter a nonequilibrium version of the NLE equation of motion. In the spirit of microrheology, NLE theory is modified to account for this based on a mechanical work like ansatz [19,20,29]:

$$F_{dyn}(r_{\perp}, \sigma; \lambda, S) = F_{dyn}(r_{\perp}, \sigma = 0; \lambda, S) - A \left( \sqrt{1 - S^{3/2}} / 2 \right) \sigma r_{\perp} \quad (6)$$

The second term on the right hand side (RHS) implies each PP step experiences an additional constant force on its center-of-mass, the magnitude of which depends on the macroscopic stress  $\sigma$ . This represents a so-called “direct” force on a PP step, and the corresponding contribution to the now nonequilibrium tube field is linear in the instantaneous PP step transverse displacement. The prefactor converting macroscopic stress to microscopic force is  $A = \pi d_T^2/4$ , i.e., the physically relevant area is taken to be set by the tube diameter [29]. A geometric “projection factor”  $\sqrt{1-S^{3/2}}/2$  enters Eq. (6) which captures the fact that the microscopic force is perpendicular to a PP step (an internal coordinate) while the macroscopic stress is defined relative to the laboratory frame; see SI for details. Using the experimental melt plateau shear modulus  $G_e = 0.0023 k_B T p^{-3}$  [30,32], the second term in Eq. (6) can be written as

$$A\left(\sqrt{1-S^{3/2}}/2\right)\sigma r_{\perp} \approx \frac{1.3\pi\sqrt{1-S^{3/2}}}{8} \frac{\sigma}{G_e} \frac{d_T^2 r_{\perp}}{d_{T,0}^3} \quad (7)$$

The first term in Eq(6) is the proper limit in the absence of this stress. It includes, if present, PP stretch and/or orientation effects, per section IIC.

In general, the stress dependence of key features of the tube confinement potential must be determined numerically. A crucial point is that for any nonzero value of  $\sigma$  the infinite barrier of the lateral confining field is formally destroyed because the maximum restoring force is finite. This results in a stress-induced *finite* entropic barrier height  $F_B$ , as shown in Fig.1(b). Furthermore, if the microscopic force  $f$  ( $\equiv A\left(\sqrt{1-S^{3/2}}/2\right)\sigma$ ) exceeds the maximum restoring force  $f_{\max}$  in  $F_{dyn}(r_{\perp}, \sigma = 0; \lambda, S)$ , then tube confinement and transverse localization is completely destroyed. This limit is called “*microscopic*

*absolute yielding*". It can always be realized in stress-controlled rheology (creep), but is not assured to be possible in startup continuous deformation which does not control stress. Regardless, the "direct force" always softens tube confinement, tends to swell the tube diameter, and reduces the transverse barrier. If the tube breaks, the corresponding transverse dynamic restoring force and barrier vanish continuously, but the transverse dynamic localization length (tube diameter) jumps from a finite to infinite value discontinuously per a simple bifurcation instability [19,29].

To treat rheology requires connections between stress, strain, strain rate, chain stretch and orientation. All these quantities are functionally coupled in a nonlinear manner to the tube confinement field, and all evolve in time or accumulated strain.

### III. Rheological Theory of Continuous Startup Shear Deformation

In our previous work [12,13] that constructed a rheological theory of entangled polymer liquids under shear deformation, several new ideas for how chains stretch and then lose "grip", the dynamics of PP contour length retraction, the impact of tube diameter fluctuations and the delayed emergence of a CCR process, have been introduced in the framework of the simplest version of the Mead-Larson-Doi (MLD) model:

$$\sigma(t) = 5G_e \lambda(t)^2 S_{xy} \quad (8)$$

$$S_{xy} = \int_{-\infty}^t dt' \frac{d\psi(t-t')}{dt'} Q_{xy} [E(t,t')] \quad (9)$$

Here,  $S_{xy}$  is the xy-component the orientation tensor,  $G_e$  is the entanglement plateau shear modulus,  $Q_{xy}$  is the affine deformation orientational factor [1],  $E$  is the

accumulated deformation, and  $\psi(t-t')$  is associated with an effective orientational relaxation time  $\tau_{eff}$  :

$$\psi(t-t') = \exp\left(-\int_{t'}^t dt'' \tau_{eff}^{-1}(t'')\right) \quad (10)$$

which includes (perturbed) reptation, CCR and perhaps activated transverse entropic barrier hopping (see section III.A).

The so-called *interchain* “grip force”  $f_{grip}$  [4,9-11], which quantifies the microscopic driving force for chains to stretch, has been formulated [12] based on the dynamic tension blob concept [33,34]. The force imbalance criterion [12] that describes when chains can begin to retract (versus affine deform) follows by equating the grip and intrachain retraction forces [12] to obtain the *mean* “loss of grip” strain,  $\gamma_{grip}$ . The existence of a broad distribution of tube diameters implies a distribution of force imbalance conditions and loss of grip strains,  $P(\gamma_{grip})$ . Then, the fraction of strands that have achieved force imbalance at a given strain can be defined as [12,13]

$$\Theta_{grip}(\gamma) = \int_0^\gamma P(\gamma_{grip}) d\gamma_{grip} \quad (11)$$

Based on our physical picture, we postulated the following evolution equation for PP contour length stretch [12,13]:

$$\frac{d\lambda}{dt} = S_{xy} \dot{\gamma} \lambda - \frac{\lambda-1}{\tau_{R,eff}} \Theta_{grip}(\gamma) \quad (12)$$

The first term describes affine stretching in the standard manner [5]. The second term describing retraction has two *qualitatively new* elements. First, it continuously “turns on” from zero with increasing elapsed time thereby capturing the amount of loss of grip (as

quantified by  $\Theta_{grip}(\gamma)$ ). Second, as grip is lost the PP contour length increasingly behaves in an unentangled manner. The chain retraction rate is faster when  $Wi_R > 1$ :

$$\tau_{R,eff}(\dot{\gamma}) = \frac{\eta(\dot{\gamma})}{G_{Rouse}} = \frac{\tau_R}{[1 + Wi_R^2]^{1/4}} \quad (13)$$

All technical details and physical arguments concerning the above concepts can be found in refs.[12,13] and SI of this article. These prior works assumed that deformation has *no* effect on the *dynamic* tube confinement field that controls transverse polymer motion. Our present central focus is to relax this assumption to include the changes of transverse/orientational dynamics due to a deformation-modified tube confinement field.

### A. Orientational Relaxation: Three Competing Processes

In prior work [12,13] we took into account two orientational relaxation processes: (i) deformation-modified reptation and (ii) *time-delayed* emergent CCR. Here we introduce a third mechanism: (iii) stress-induced transverse barrier hopping. We also generalize our treatment of (i) to include deformation-induced changes of the tube.

For (i), we explore the idea that the reptation time is directly related to the tube diameter as true for rod liquids [19,20] and chains in equilibrium:  $\tau_{rep}/\tau_{rep,0} = (d_{T,0}/d_T)^2$ , where  $\tau_{rep,0}$  is the equilibrium reptation time associated with orientational relaxation,  $\tau_{rep,0} = 3Z\tau_{R,0}$ . Reptation speeds up (slows down) if the tube swells (shrinks), and the latter depends on time or strain. For (ii) we argued [13] CCR is present only once the irreversible process of PP contour length reduction has begun which occurs beyond the stress overshoot for all  $Wi_R$  [13]. The effective orientational relaxation rate is then:

$$\tau_{eff}^{-1} = \tau_{rep}^{-1} + \beta_{CCR} \left( \frac{\lambda_{max} - \lambda}{\tau_{R,eff}} \right) \Theta_+ \left( \gamma > \gamma(\lambda_{max}) \right) \quad (14)$$

The parameter  $\beta_{CCR}$  encodes the physical intuition [5] that CCR is less effective when chains stretch; following others,  $\beta_{CCR}$  is taken to be inversely proportional to  $\lambda$  [5].

The third relaxation channel is stress-assisted transverse entropic barrier hopping. Its characteristic relaxation time is straightforward to compute using Kramers theory for rigid rod liquids where there is only one dynamic free energy (or in other words one PP step) and the rod CM displaces rigidly [19,20]. However, for chains there is a dynamic free energy present for each of the  $Z$  connected PP steps that define a flexible polymer (Fig.1(a)). Hence, to treat hopping one cannot a priori ignore chain connectivity, and treating this aspect is a difficult and unsolved problem for entangled polymers. It is reminiscent of classic work by Helfand and Skolnick [35] on trans-gauche conformational transitions in polymer melts where one large amplitude activated torsional hopping over a barrier motion can occur only due to many much smaller scale correlated motions in the trans wells of nearby connected bonds. Moreover, the precise amount of global chain orientation relaxed by one PP step level hop is a complex issue. Thus, due to these uncertainties, when calculating the barrier hopping time  $\tau_{hop}$  we consider two naive extreme ansatzes. A common constraint is the hopping time must reduce to the unentangled chain orientational relaxation time,  $\tau_{R,eff}$ , if there is no tube.

The simplest assumption for the mean hopping time is  $\tau_{hop} \approx \tau_{R,eff} \exp(\beta F_B)$ , which is presumably a lower bound since only one PP step transverse barrier enters

(chain connectivity is ignored when describing the transverse hop). The net orientational relaxation rate then becomes:

$$\tau_{eff}^{-1} = \tau_{rep}^{-1} + \tau_{hop}^{-1} + \beta_{CCR} \left( \frac{\lambda_{max} - \lambda}{\tau_{R,eff}} \right) \Theta_+ \left( \gamma > \gamma(\lambda_{max}) \right) \quad (15)$$

But if a hop involves simultaneously surmounting even a few PP barriers the time scale could become much longer. Thus, the other extreme model we study is to assume that chain connectivity results in a PP step hopping time that is so long as to be effectively infinite, corresponding to adopting Eq.(14).

### B. Orientational Order Parameter Dynamics

The PP level scalar nematic order parameter,  $S$ , varies from 0 to 1 for unoriented to fully uniaxially oriented PP steps under shear deformation. While it plays no direct role in standard tube models of rheology, in our approach it enters since all aspects of the dynamic free energy depend on chain orientation. However,  $S$  does not enter explicitly in our rheological calculation of stress. The dynamical evolution equation governing  $S$  is a competition between relaxation-driven orientational randomization and a mechanically-driven, rate-dependent, orientational driving force [19]. Given the d-PP model adopted and our use of the independent alignment assumption (IAA) to compute stress, for simplicity and consistency we adopt the same description of its dynamics developed for entangled rod fluids which corresponds to the evolution equation [19]:

$$\frac{dS(t)}{dt} = \frac{-S(t)}{\tau_{eff}} + \left( \frac{dS_a}{d\gamma} \Big|_{\gamma=\gamma_{eff}} \right) \dot{\gamma} \quad (16)$$

The previously developed concept of an effective strain [19],  $\gamma_{eff}$ , is employed, which satisfies  $S_a(\gamma_{eff}) = S(t)$ . Physically,  $S_a$  in Eq. 16 is the PP step orientational order

parameter due to "strain in affine motion". As for rods, we assume that under affine conditions the Lodge-Meissner relation [1] applies:

$$S_a = \frac{-2\gamma}{\gamma - 3\sqrt{\gamma^2 + 4}} \quad (17)$$

and this functional form applies in an effective sense beyond the affine regime [19].

### C. Summary of Theory and Its New Physical Aspects

Only two parameters enter: number of entanglements,  $Z \equiv N/N_e$ , and Weissenberg or Rouse Weissenberg number,  $Wi = \dot{\gamma}\tau_{rep,0}$  or  $Wi_R = \dot{\gamma}\tau_{R,0}$ , respectively. Equations (8), (9), (12), (14) (or (15)) and (16) form a closed set of coupled nonlinear equations which govern the evolution of an entangled polymer liquid under continuous startup shear deformation. There are three dynamic structural variables: stretch ratio  $\lambda$ , dynamic tube diameter  $d_T$  and orientational order parameter  $S$ .

Compared to our prior work [12,13] two new physical aspects enter. (i) Deformation-induced changes of the tube field via the "direct force" or indirectly via PP orientation and stretch. This modifies the reptation time and introduces the new transverse hopping relaxation channel. (ii) The accompanying *dynamic* tube diameter  $d_T$ , transverse entropic barrier  $F_B$ , and  $S$  all dynamically evolve with time or strain in a manner that is dynamically coupled with the full rheological response.

We will show that points (i) and (ii) result in rheological predictions that are different compared to our previous theory [12,13] if  $Wi_R < 1$  due to the dominance of  $S_y$  which is significantly affected by perturbed reptation and perhaps transverse barrier hopping. Some of our rheological results are compared with experiments and simulation.

However, our prior results [12,13] under fast deformation conditions ( $Wi_R > 1$ ) summarized below remain virtually unchanged due to the dominance of chain stretch. This is a nontrivial prediction, and is a deduction, not an assumption. Furthermore, the dynamical structural information (dynamic tube diameter, PP step order parameter, transverse barrier, etc), not treated at all in prior work [12,13], are of interest in their own right in addition to their possible influence on rheology. Our new predictions for these dynamical structural properties should be testable in future simulations and experiments.

#### IV. Rheological and Chain Dynamical Results

We first summarize as relevant background key prior results [12,13] when  $Wi_R > 1$ . (i) The stress undershoot coordinates follow apparent power laws:  $\gamma_{undershoot} \propto Wi_R^{0.3}$ ,  $\sigma_{undershoot}/G_e \propto Wi_R^{0.32}$ . (ii) An apparent fractional power law growth of the steady state stress  $\sigma_{ss}/G_e \propto Wi_R^{0.30}$ . (iii) The chain stretch ratio in the steady state grows as  $\lambda_{ss} \propto Wi_R^{0.31}$ . (iv) The steady state  $S_{xy}$  obeys  $S_{xy}^{ss} \propto Wi_R^{-0.30}$ . (v) The steady-state effective relaxation time follows a nearly Z-independent inverse power law,  $\tau_{eff}^{ss} \propto Wi_R^{-0.6}$ . (vi) At the stress overshoot,  $\sigma_{max}/G_e \propto Wi_R^{0.3}$  and  $\gamma_{max} \propto Wi_R^{0.3}$ . Very similar overshoot scaling laws were experimentally found by Wang et al. in solutions and melts [4,11,14] and then confirmed by another experiment [15] and simulation [16]. (vii) The chain stretch ratio at the stress overshoot scales as  $\lambda_{overshoot} \propto Wi_R^{0.29}$ .

We find in our new work that all of the above results remain virtually unchanged since when chains stretch the tube field hardens (high transverse entropic barrier  $F_B$ , see Sec. V), and the orientational relaxation via barrier hopping can be neglected and is rather

dominated by CCR beyond the stress overshoot. Furthermore, the importance of orientational relaxation for the stress overshoot is small when  $Wi_R > 1$ . Given this, the primary focus below is the *slow nonlinear regime*,  $Wi_R \leq 1$  and  $Wi > 1$ .

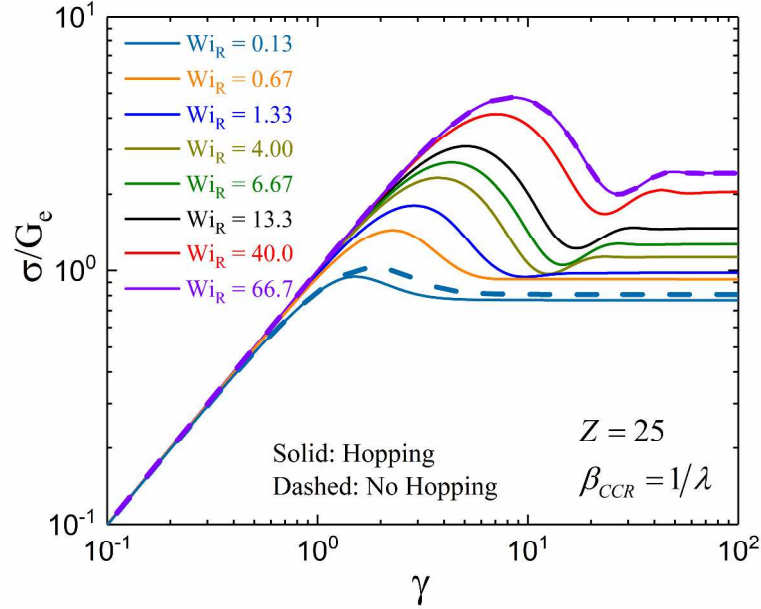


**Figure 3** Dimensionless shear stress as a function of strain at increasing dimensionless deformation rates (bottom to top) for  $Z = 25$  and  $\beta_{CCR} = 1/\lambda$ . Solid curves include the transverse hopping process (Eq. (15)) and dashed curves do not (Eq. (14)).

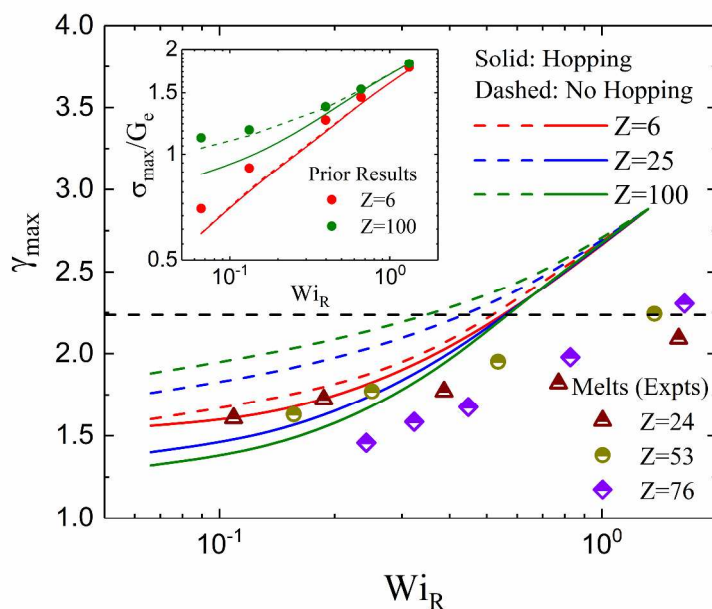
### A. Full Stress-Strain Response

Figure 3 shows representative calculations for  $Z = 25$  of the total stress (normalized by the equilibrium entanglement plateau modulus) plotted as a function of strain for different dimensionless shear rates ( $Wi_R < 1$  and  $Wi_R > 1$ ) with  $\tau_{eff}$  calculated using  $\beta_{CCR} = \lambda^{-1}$  with Eq. (14) or (15). Basic features include a stress overshoot and emergence at high enough  $Wi_R$  of a stress undershoot(s), which both grow in amplitude

with increasing shear rate. The overshoot strain does vary with shear rate when  $Wi_R < 1$ , and even more strongly when  $Wi_R > 1$ . Comparing the results using Eq. (14) or (15) one sees that the transverse barrier hopping process modestly affects the stress-strain curve at low  $Wi_R$ , but its influence can be neglected at high  $Wi_R$ .

### B. Stress Overshoot Behavior

The stress overshoot is specified by its coordinates  $\sigma_{\max}$  and  $\gamma_{\max}$ . Predictions for the overshoot strain,  $\gamma_{\max}$ , are shown in Figure 4. At low deformation rates  $Wi_R < 1$ , our prior theory [12,13] predicted an essentially rate-independent  $\gamma_{\max} \approx 2.25$ . However, including deformation-dependent reptation and hopping (using Eq.(15)) leads to an increase of the overshoot strain with shear rate when  $Wi_R < 1$ . From careful examination of the figure one sees it varies from  $\gamma_{\max} \sim 1.3-2.2$  (solid curves). This is due to the deviation of the orientational relaxation time from the DE prediction, which affects  $S_{xy}$  in Eq. (9). Specifically, when  $Wi_R < 1$ , if the shear rate is not sufficiently small the maximum value of  $S_{xy}$  no longer occurs at  $\sim 2.25$ , but varies with  $Wi_R$  in a way consistent with the stress overshoot strain. A constant strain value of  $\sim 2.25$  is only recovered for small enough shear rate; for example, when  $Wi_R < 0.01$  if  $Z=100$ . The stress overshoot strain  $\gamma_{\max}$  at low  $Wi_R$  also decreases with  $Z$ , mainly because the barrier (and hopping time) is lower for larger  $Z$  at the same  $Wi_R$ , which accelerates orientational relaxation.



**Figure 4** Strain at the stress overshoot as a function of Rouse Weissenberg number for three degrees of entanglement  $Z = 6, 25, 100$ . Solid and dashed curves represent the results with the hopping process (Eq. (15)) and without the hopping process (Eq. (14)), respectively. The black dashed horizontal line is the Doi-Edwards prediction which is relevant for  $Wi_R < 1$  in the absence of chain stretch. Experimental results [4,14] for three SBR melts (half-filled symbols) are also indicated. Inset: the corresponding dimensionless overshoot stress for  $Z = 6$  and 100. “Prior Results” (filled circles) are those obtained from the theory [12,13] which ignored tube deformation.

The SBR melt data of Wang et al. [4,14] for the overshoot strain is also shown in Fig.4. Gross trends are the overshoot strain (a) increases with shear rate, (b) can be well below the DE value of  $\sim 2.25$ , and (c) roughly appears to become smaller as  $Z$  increases. These trends are qualitatively consistent with our theoretical results. Similar trends are found in the experiments of Auhl et al. on polyisoprene liquids [36], although the

variation with rate and  $Z$  of the reported data is significantly less distinct. More high precision experimental measurements of the overshoot strain would be valuable.

Figure 4 also shows the corresponding theoretical results (dashed curves) if transverse hopping is ignored (Eq.(14)) in computing  $\tau_{eff}$ . A similar rate dependence of the overshoot strain is found as when hopping is included. However, the  $Z$ -dependence is the opposite. This further motivates performing new high precision measurements. Note that once  $Wi_R > 1$ , our results for all  $Z$  values converge to a single curve, which agrees with prior work [12,13] based on assuming no changes of the tube field with deformation.

The inset of Figure 4 shows calculations of the overshoot stress,  $\sigma_{max}$ , which monotonically grows with increasing  $Wi_R$  and  $Z$ . Including transverse hopping only weakly reduces its magnitude, and less so as  $Z$  grows. Such  $Wi_R$  and  $Z$  dependences for  $\sigma_{max}$  are qualitatively consistent with the Auhl et al. experiments [36]. Also shown are our prior results [12,13], and the trends are qualitatively identical as here. Quantitatively, ignoring tube deformation leads to larger overshoot stresses, ala the overshoot strain behavior. The reason is ignoring tube dilation and/or barrier hopping increases the orientational relaxation time, which shifts the overshoot to larger strain and stress.

As far as we are aware, there are no definitive published simulations for the question of whether for slow nonlinear deformations the overshoot coordinates change in a non-negligible and systematic manner with shear rate and  $Z$ . Such simulations would be very valuable to test our results. For that purpose we report our numerical predictions for typical shear rates and low  $Z$  values typically studied using simulation. For  $Wi_R = (0.25, 0.5, 1)$ , based on including hopping we predict for  $Z=6$  overshoot strains of (1.8, 2.2,

2.7), while if hopping is ignored they are (1.9, 2.2, 2.7). The effect of hopping is very tiny, but it does matter for the qualitative variation of the overshoot strain with  $Z$ .

### C. Effective Orientational Relaxation Time and Barrier Hopping

The effective orientational relaxation time is a fundamental quantity affected by changes of the tube confinement field that, in turn, can modify rheological response. Strong acceleration of relaxation is generically predicted, which is more pronounced as  $Wi_R$  increases [12,13]. At low deformation rates  $Wi_R < 1$ , there is a noticeable influence of a changing tube field on the effective orientational relaxation time.

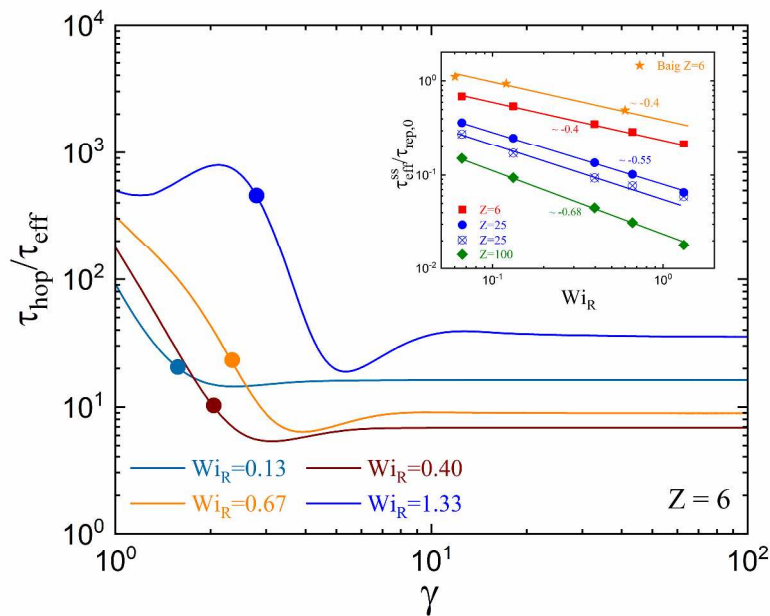


**Figure 5** Log-log plot of the transverse barrier hopping time normalized by the effective orientational relaxation time as a function of strain for  $Z=6$  and four low shear rates. Dots indicate the strains at the stress overshoot. Inset: Log-log plot of the steady state effective orientational relaxation time normalized by the equilibrium reptation time as a function of Rouse Weissenberg number. The orange stars are the orientational relaxation time data

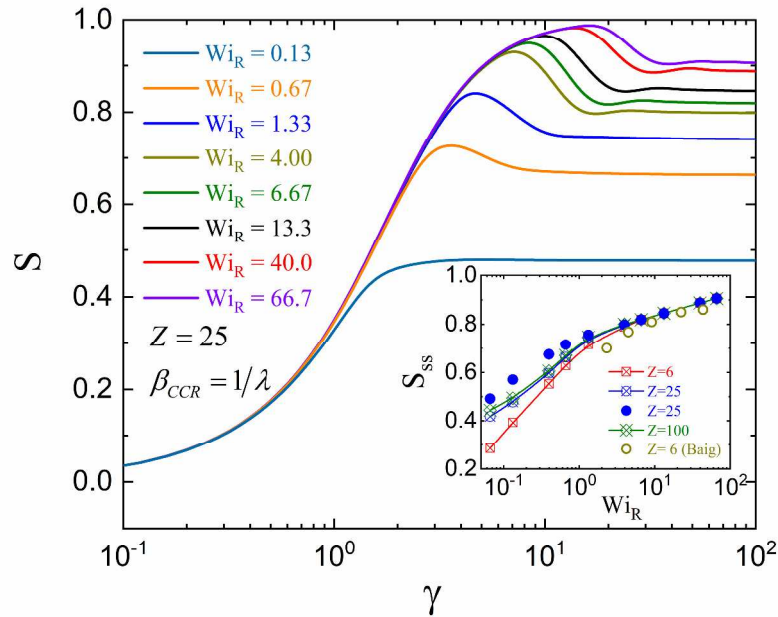
from the simulation of Baig et al. for  $Z=6$  [37]. Cross symbols are the theoretical results with the hopping process (Eq. (15)) and filled symbols the results without hopping (Eq. (14)). Effective power law scaling exponents are indicated.

Figure 5 shows how important transverse hopping is (within the model of Eq.(15)) compared to perturbed reptation and CCR for orientational relaxation. The mean hopping time divided by the effective total orientational relaxation time is plotted as a function of strain for various dimensionless rates and two  $Z$  values. For  $Wi_R > 1$  the hopping process is generically not competitive (far too large to matter for all  $Z$  and strain values). This is because chain stretching hardens the tube and increases the transverse barrier, as discussed in section V. For slow nonlinear deformations, one sees for the lightly entangled  $Z=6$  system that with increasing strain approaching the overshoot the hopping time becomes more important in a relative sense, but is always nearly an order of magnitude longer than the effective orientational relaxation time. Hopping is most important slightly beyond the stress overshoot strain, as indicated by the dots on the Figure 5 curves. We conclude the tube is dynamically stable for low  $Z$  in that transverse hopping is unimportant, a conclusion which explains the  $Z=6$  results in Fig.4. However, for  $Z=25$  (see SI, Figure S2), although the trends with shear rate and strain of the time scale ratio remain the same as for  $Z=6$ , the absolute importance of transverse hopping is significantly larger. As discussed in section V, this is because the transverse barrier is smaller for bigger  $Z$  since  $S$  is larger at the same  $Wi_R < 1$ . Enhanced importance of hopping is the origin of the different trends with  $Z$  of our results for the overshoot coordinates in Fig.4.

The inset of Figure 5 shows typical effective orientational relaxation time results in steady state (ss). Our prior theory [12,13] found over a limited regime that  $\tau_{eff}^{ss}$  decreases with  $Wi_R$  as an apparent power law with an exponent that becomes steeper with increasing  $Z$ , varying from  $\sim -0.64$  to  $\sim -1.0$  for  $Z = 6-100$ . However, the decrease of  $\tau_{eff}^{ss}$  with shear rate becomes slower when using Eq. (14) to calculate the effective orientational relaxation time, and the scaling exponent varies from  $\sim -0.4$  to  $\sim -0.68$  for  $Z = 6-100$ . This agrees with simulation at low  $Z=6$  [37,38], as shown in Fig.5. In addition, Fig.5 shows that while the transverse hopping process reduces the effective relaxation time, the power law scaling in the narrower regime remains almost identical. We mention that simulations by different groups [37,38] give quite different effective relaxation times in the narrow region of  $0.05 < Wi_R < 1$  shown in Figure 5.

#### **D. Nematic PP Orientational Order Parameter**

The deformation-induced PP step orientational order parameter,  $S$ , is an important property. Physically, one expects alignment reduces the probability of PP segment collisions, leading to less entanglement, and hence tube dilation and enhanced transverse motion. The latter in turn affects relaxation-driven orientational randomization (first term on right side of Eq. (16)). Hence,  $S$  is coupled with the effective orientational relaxation time. Results for  $Z = 25$  are shown in the main frame of Figure 6 during deformation based on Eq.(15) (includes hopping). One sees that  $S$  goes through a maximum and decreases when  $\tau_{eff}$  begins to drop due to emergent CCR. Significant orientation develops well before the chains begin to stretch significantly.



**Figure 6** PP step orientational order parameter as a function of strain at increasing deformation rates (bottom to top) for  $Z = 25$ . The hopping process (Eq. (15)) is included. Inset: PP step nematic orientational order parameter in the steady state as a function of Rouse Weissenberg number for 4 values of degrees of entanglement. Cross and filled symbols are results with the hopping process (Eq. (15)) and without hopping process (Eq. (14)), respectively. The open circles in the inset are simulation results for the chain orientational order parameter of a model with  $Z=6$  [37].

Calculations of the orientational order parameter in the steady state,  $S_{ss}$ , are shown in the inset of Figure 6, which monotonically grows with shear rate. At low  $Wi_R < 1$ ,  $S_{ss}$  increase rapidly, while for  $Wi_R > 1$ , they slowly increase with  $Wi_R$ . Although  $S_{ss}$  is quite insensitive to  $Z$  at high  $Wi_R > 1$ , noticeable differences at low  $Wi_R < 1$  are predicted: a larger  $Z$  leads to larger  $S_{ss}$  for a fixed  $Wi_R < 1$ . The influence of hopping is

also indicated in the inset of Figure 6. It reduces  $S$  at low  $Wi_R < 1$  because of stronger relaxation-driven orientational randomization. The corresponding quantity at the stress overshoot (Fig. S3 of SI),  $S_{overshoot}$ , shows very similar dependences on shear rate and  $Z$ .

Also shown in the inset of Figure 6 are steady state MD simulation results of Baig et al. [37] for a lightly entangled melt with  $Z=6$ . Results are shown only in the fast deformation regime because what has been measured in simulation is the nematic orientational order parameter defined at the full chain scale, while our calculations are at the PP step level. These two measures of orientation are not independent, but are not the same. They are expected to be different in slow deformations where there is almost no stretching. At high shear rates where chains strongly stretch and align, we believe it is fair to compare them. Since we employ a disconnected PP model, one expects stronger alignment than in simulation, as we find. The inset of Figure 6 shows rather good agreement between theory and simulation, which improves as the shear rate gets larger.

#### D. Dynamic Tube Diameter

The evolution of the *dynamic* tube diameter (an emergent transverse localization length) is functionally coupled to stress, chain stretch ratio and  $S$  (see. Eq. (6)). Figure 7 shows a complex non-monotonic variation with strain. The strain at the stress overshoot, the strain at the maximum chain stretch ratio, and the strain at the maximum value of  $S$  are all indicated in Figure 7. The local maximum of the tube diameter occurs close to where  $S$  is a maximum since polymer orientation reduces entanglement, which occurs just beyond the strain of maximum chain stretch. At low deformation rates, because stretching can be neglected, tube dilation is always observed, which speeds up reptation-driven orientational relaxation. In contrast, at very high deformation rate, the tube

diameter is predicted to be compressed due to the dominant effect of chain stretch. For intermediate deformation rates, the tube diameter can be compressed or dilated depending on the transient stress, stretch ratio and orientational order parameter.

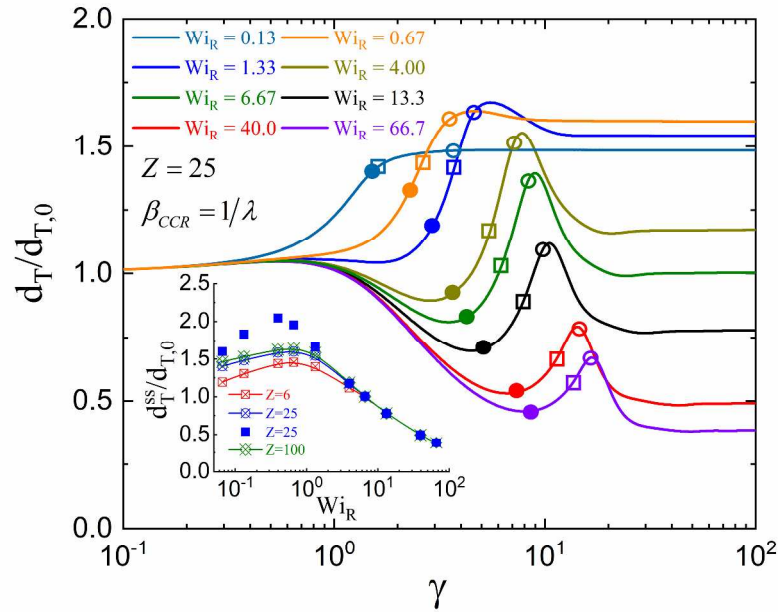


**Figure 7** Dynamic tube diameter (normalized by its equilibrium value) as a function of strain for increasing deformation rates (top to bottom) and  $Z = 25$ . The hopping process (Eq. (15)) is included. The strain at the stress overshoot (filled circles), the strain at maximum chain stretch ratio (open squares), and the strain at maximum orientation order parameter (open circles) are indicated. Inset: The corresponding results in the steady state plotted as a function of Rouse Weissenberg number for 4 values of degree of entanglement. Cross symbols are results with hopping and filled symbols ignore hopping.

The tube diameter in the steady state are shown in the inset of Figure 7. The predicted crossover from “tube softening” to “tube hardening” again demonstrates that while chain stretch compresses the tube at high shear rates, the tube dilates with growing

orientation and stress at low shear rates. This tube widening with increasing shear rate at low  $Wi_R$  is qualitatively similar to that previously predicted for entangled rod solutions [19] due to the dominance of orientational dynamics. The inset of Figure 7 also indicates that including activated hopping only modestly decreases tube dilation at low  $Wi_R < 1$  and leads to no new qualitative behaviors. The tube diameter at the stress overshoot (Figure S4 of SI) shows very similar dependences on deformation rate and  $Z$ .

Finally, we emphasize that, per deGennes' original conception [2], the tube diameter in our theory is an explicitly dynamical property (transverse localization length). Thus, our result in Fig.7 that when chains stretch enough in fast deformations the tube diameter shrinks makes physical sense, i.e. less transverse *dynamic* fluctuations. This does not contradict our prediction of net faster dynamics, shear thinning, etc. when chains stretch and orient. In this regard, we emphasize that comparisons of our results to nonequilibrium simulations that employ *static geometric* PP contour length reduction algorithms [32,37-40] should be done with caution. Though seemingly (empirically) valid in equilibrium, the validity (or physical meaning) of such PP contour length reduction algorithms out of equilibrium is unclear to us. While the *dynamic* tube diameter in our theory can be compressed at high deformation rate due to chain stretch, PP contour length reduction algorithms always predict tube dilation under deformation. Importantly, O'Connor, Alvarez and Robbins [41] have very recently used MD simulation to measure the *dynamic* tube diameter based on the time-dependent deviation of monomers from primitive path during uniaxial extension. They find this dynamic tube diameter can decrease significantly at high deformation rate, in qualitative accord with our picture.

Also, our prediction of dynamic tube diameter compression is not inconsistent with the idea that deformation promotes disentanglement, faster relaxation, and lower viscosity.

## V. Transverse Tube Field Stability and Entropic Barrier Heights

The transverse entropic barrier  $F_b$  is the key feature of the tube confinement field that quantifies its dynamic stability. Under equilibrium conditions the barrier is predicted to be infinite. This seems in the spirit of the naive view of an unbreakable (infinitely strong) tube or entanglement network per a chemically crosslinked rubber. However, since NLE theory predicts the tube has a finite strength, if stress is nonzero the barrier height becomes finite [19,20,29] and hence dynamic tube stability is not assured.

Figure 8 shows  $F_b$  for a  $Z = 25$  melt as a function of strain for different shear rates ( $Wi_R < 1$  and  $Wi_R > 1$ ) including the hopping process when computing  $\tau_{eff}$  (Eq. (15)). For strains well below the overshoot, the barriers remain very high and the tube is thus expected to be stable. Its dramatic drop at higher strain when  $Wi_R < 1$  is due to the large increase of stress and orientation, while the PP contour length remains unstretched. Decrease of the transverse barrier effectively turns on a competing hopping process where the lateral tube confinement barrier can potentially be dynamically surmounted.

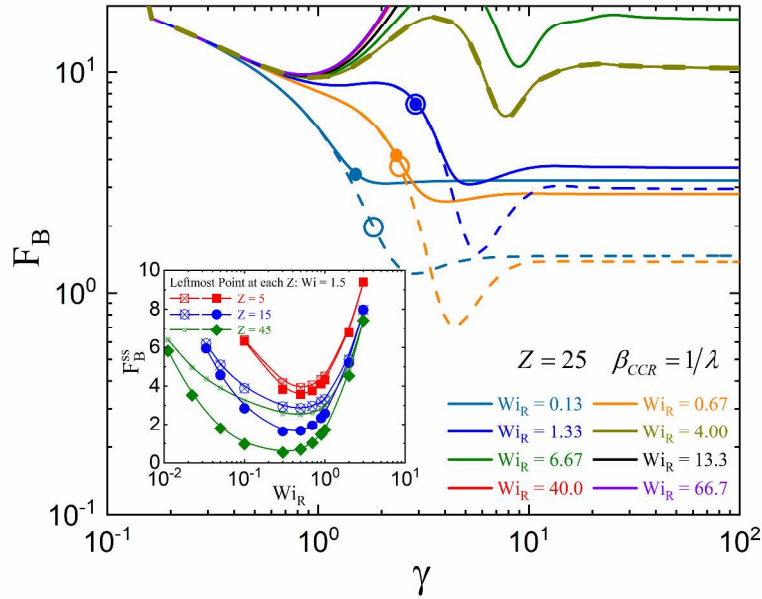


**Figure 8** Transverse entropic barrier in units of the thermal energy as a function of strain for  $Z = 25$  at various dimensionless shear rates. Solid curves are results with the hopping process and dashed curves the results without the hopping process. The strains at the stress overshoot with hopping (filled circles) and without hopping (open circles) for the lowest three  $Wi_R$  systems are indicated. Inset: Transverse entropic barrier in units of the thermal energy in the steady state as a function of dimensionless shear rate for  $Z = 5, 15$  and  $45$ . Cross symbols are results with the hopping process and filled symbols results without hopping process. Curves are a guide to the eye.

On the other hand, when  $Wi_R > 1$  the barrier is much larger than when  $Wi_R < 1$  due to the predicted hardening effect of chain stretch on tube confinement. As a consequence, the hopping process can be safely ignored. Like the dynamic tube diameter, the non-monotonic variation of the transverse barrier is due to a subtle competition between varying transient shear stress, PP stretch ratio and orientational order. Before

approaching the steady state, we always find a minimum transverse barrier for both  $Wi_R < 1$  and  $Wi_R > 1$  that appears at a strain modestly beyond the stress overshoot at  $\gamma_{\max}$ .

For comparison, analogous results based on not allowing hopping (using Eq. (14)) are also shown in Fig. 8. One sees that hopping is important only below or around  $Wi_R = 1$ , and it increases  $F_B$ , including its minimum and steady state values. These trends can be mainly attributed to the decrease of  $S$  due to hopping (see Fig. 6). In addition, the minimum barrier height gets smaller when using Eq. (14) (no hopping) to compute  $\tau_{eff}$ .

Calculations of the transverse entropic barrier at steady state,  $F_B^{ss}$ , are shown in the inset of Fig. 8 based on Eq.(15). As relevant background, we also calculated the flow curve for four degrees of entanglement which span the weakly to heavily entangled range,  $Z=5, 15, 25, 45$  (see Figure S5 of SI). Four key trends are seen in the inset of Fig.8. 1)  $F_B^{ss}$  at low  $Wi = 1.5$  is relatively high ( $\approx 6$ ) and  $Z$ -independent. 2)  $F_B^{ss}$  non-monotonically varies with shear rate, achieving a minimum when  $Wi_R \approx 0.5$  which occurs in the stress plateau region of the flow curve close to its inflection point [13]. 3) When  $Wi_R > 1$ , where the system is beyond the upper end of the stress plateau region and the steady state stress grows with shear rate [13], the steady-state transverse barrier grows rapidly with deformation rate. 4) At the same value of  $Wi_R$ ,  $F_B^{ss}$  is larger for smaller  $Z$ . The reason is that at fixed  $Wi_R$ , less entanglement means smaller  $Wi$ , and hence smaller  $S$ , per Fig. 6.

Representative results using Eq. (14) are also included in the inset of Fig. 8. The rate and  $Z$  dependences of  $F_B^{ss}$  become stronger, mainly due to the difference of  $S$  (see Fig. 6). However, all the qualitative trends are unaffected.

Finally, we speculate there might be a connection between the vanishing of microscopic transverse barrier, which signals the deformation-induced collapse of transverse chain localization, and the tendency of entangled liquids to macroscopically shear band [42-46]. But this topic is beyond the scope of the present article.

## VI. Discussion

We have generalized our new theory for the startup continuous shear rheology of entangled chain liquids [12,13] to address the consequences of a deformation-induced anharmonic tube field at the PP step level. Numerical results for the stress-strain curves, effective orientational relaxation time, nematic orientational order parameter, dynamic tube diameter and transverse entropic barrier under nonequilibrium conditions were presented as a function of dimensionless shear rate, strain and degree of entanglement.

Compared to our prior results [12,13] based on the assumption that the tube confinement field is not modified by deformation, the effect of a deformation-dependent anharmonic tube confinement field on rheology at high shear rates  $Wi_R > 1$  can be essentially ignored; all effective scaling power laws with  $Wi_R$  remain virtually unchanged. The reason is the dominance of the chain stretch and CCR and irrelevance of perturbed reptation and transverse activated barrier hopping.

However, in close connection with prior work on entangled rod solutions [19], the deformation-modified tube confinement field can significantly affect the rheological response when  $Wi_R < 1$  where chains remain essentially unstretched and orientational dynamics dominates. In contrast to the almost rate-independent strain at the stress overshoot ( $\gamma_{\max}$ ) at low  $Wi_R < 1$  found previously [12,13],  $\gamma_{\max}$  now increases in the

range of  $\sim 1.3-2.2$  as  $Wi_R$  grows because there are shear rate and  $Z$  dependent changes of the perturbed reptation time and transverse barrier hopping time. Such behavior of  $\gamma_{\max}$  is qualitatively consistent with some experiments [4,14,36]. New simulations are highly desirable to further test our results. Deformation-induced changes of the tube field also modify the apparent scaling behavior of the effective orientational relaxation time when  $Wi_R < 1$ . The tube diameter and transverse entropic barrier are rich functions of strain, shear rate and degree of entanglement. Deformation can increase or decrease the tube diameter, and the non-monotonic changes with strain are possible due to competition between the effects of PP orientation, PP stretch, and the direct effect of stress.

We have introduced the possibility that stress-assisted activated hopping of PP segments orthogonal to their axis (a local dynamical "tube-breaking" event) may be important for the nonlinear rheological response. However, theoretical treatment of this new mechanism is very difficult, and quantification of a hopping rate was done in the present article in a crude manner. It is highly desirable to more directly probe the relevance of this idea to entangled polymer liquids under *slow nonlinear* deformation using experiment (e.g., chain labeling scattering methods) or simulation. Possible experimental and/or computational ways forward might be as follows. (i) Measure the dynamic PP segment mean square displacement (MSD) as a function of time on the fly for slow nonlinear deformations ( $Wi_R < 1$ ). Hopping should modify the time evolution of this quantity in the direction of enhanced amplitude relative to classic tube models. (b) Neutron spin echo or simulation measurements of the single chain coherent dynamic structure factor under deformation as a function of time and wavevector. (c) Measurement of the dynamic van Hove function for the transverse PP motion might

reveal large non-gaussian signatures indicative of activated hopping events in analogy to studies of glassy forming systems. At the moment we do not have precise predictions for the observables of such experiments and/or simulations, but obtaining them may be a future tractable goal.

Finally, our basic approach can be extended to treat extensional rheology, including the nature of the grip force [4,9], engineering versus Cauchy stress response [47,48], and whether molecular-scale deformation effects can effectively destroy the entanglement network which may serve as a nucleating event to trigger macroscopic instabilities such as tensile and brittle fracture and necking [49,50]. Work is in progress in these directions.

**Acknowledgement.** This work was supported by the U.S. Department of Energy, Office of Science, Basic Energy Sciences, Materials Sciences and Engineering Division. Helpful discussions with Shi-Qing Wang, Yangyang Wang, Zhen-Gang Wang, Dimitris Vlassopoulos, Hiroshi Watanabe and Charles Schroeder are gratefully acknowledged.

## References

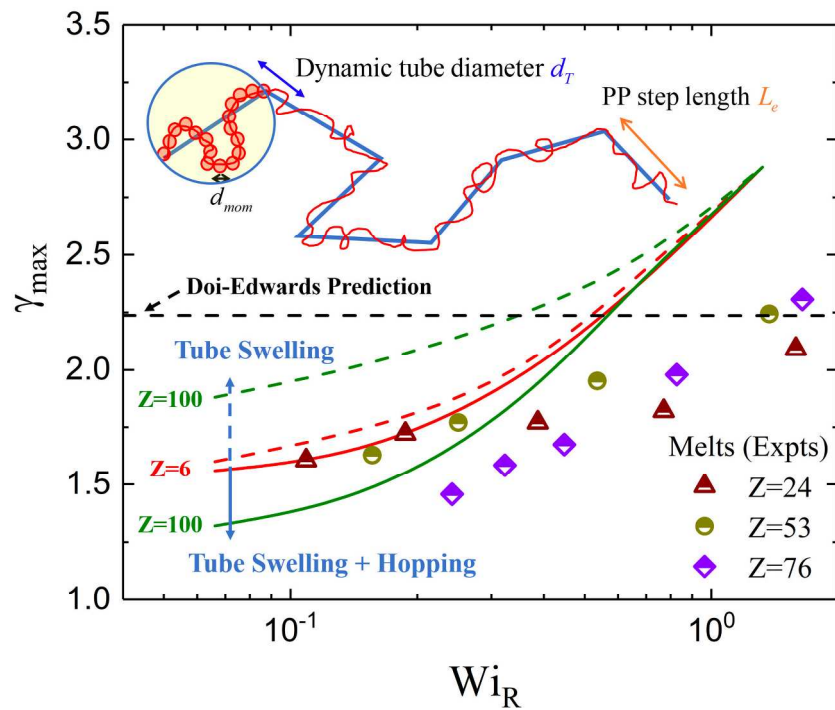
- (1) M. Doi and S. F. Edwards, *The Theory of Polymer Dynamics*, Clarendon Press, Oxford, 1986.
- (2) P. G. de Gennes, *J. Chem. Phys.*, 1971, **55**, 572.
- (3) T. C. B. McLeish, *Adv. Phys.*, 2002, **51**, 1379.
- (4) S.-Q. Wang, *Nonlinear Polymer Rheology: Macroscopic Phenomenology and Molecular Foundation*, Wiley, Hoboken, NJ, 2018.

- (5) D. W. Mead, R. G. Larson and M. Doi, *Macromolecules*, 1998, **31**, 7895.
- (6) R. S. Graham, A. E. Likhtman, T. C. B. McLeish and S. T. Milner, *J. Rheol.* 2003, **47**, 1171.
- (7) Z. Wang, C. N. Lam, W.-R. Chen, W. Wang, J. Liu, Y. Liu, L. Porcar, C. B. Stanley, Z. Zhao, K. Hong and Y. Wang, *Phys. Rev. X*, 2017, **7**, 031003.
- (8) W.-S Xu, J. M. Y. Carrillo, C. N. Lam, B. G. Sumpter and Y. Wang, *ACS Macro Lett.*, 2018, **7**, 190.
- (9) S.-Q. Wang, S. Ravindranath, Y. Wang and P. Boukany, *J. Chem. Phys.*, 2007, **127**, 064903.
- (10) S.-Q. Wang, Y. Wang, S. Cheng, X. Li, X. Zhu and H. Sun, *Macromolecules*, 2013, **46**, 3147.
- (11) Y. Wang and S.-Q. Wang, *J. Rheol.*, 2009, **53**, 1389.
- (12) K. S. Schweizer and S.-J. Xie, *ACS Macro Lett.*, 2018, **7**, 218.
- (13) S.-J. Xie and K. S. Schweizer, *Macromolecules*, 2018, **51**, 4185.
- (14) P. E. Boukany, S.-Q. Wang and X. Wang, *J. Rheol.*, 2009, **53**, 617.
- (15) S. Costanzo, Q. Huang, G. Ianniruberto, G. Marrucci, O. Hassager and D. Vlassopoulos, *Macromolecules*, 2016, **49**, 3925.
- (16) J. Cao and A. E. Likhtman, *ACS Macro Lett.*, 2015, **4**, 1376.
- (17) S. Jeong, J. M. Kim and C. Baig, *Macromolecules*, 2017, **50**, 3424.
- (18) C. Baig, V. G. Mavrantzas and M. Kröger, *Macromolecules*, 2010, **43**, 6886.
- (19) D. M. Sussman and K. S. Schweizer, *Macromolecules*, 2013, **46**, 5684.
- (20) D. M. Sussman and K. S. Schweizer, *Macromolecules*, 2012, **45**, 3270.
- (21) D. M. Sussman and K. S. Schweizer, *Phys. Rev. Lett.*, 2011, **107**, 078102.

- (22) K. S. Schweizer and E. J. Saltzman, *J. Chem. Phys.*, 2003, **119**, 1181.
- (23) K. S. Schweizer, *J. Chem. Phys.*, 2005, **123**, 244501.
- (24) T. T. Falzone and R. M. Robertson-Anderson, *ACS Macro Lett.*, 2015, **4**, 1194.
- (25) T. T. Falzone, S. Blair and R. M. Robertson-Anderson, *Soft Matter*, 2015, **11**, 4418.
- (26) C. D. Chapman and R. M. Robertson-Anderson, *Phys. Rev. Lett.*, 2014, **113**, 098303.
- (27) D. M. Sussman and K. S. Schweizer, *Phys. Rev. Lett.*, 2012, **109**, 168306.
- (28) D. M. Sussman and K. S. Schweizer, *J. Chem. Phys.*, 2013, **139**, 234904.
- (29) K. S. Schweizer and D. M. Sussman, *J. Chem. Phys.*, 2016, **145**, 214903.
- (30) L. J. Fetters, D. J. Lohse, D. Richter, T. A. Witten and A. Zirkel, *Macromolecules*, 1994, **27**, 4639.
- (31) R. Everaers, *Phys. Rev. E*, 2012, **86**, 022801.
- (32) R. Everaers, S. K. Sukumaran, G. S. Grest, C. Svaneborg, A. Sivasubramanian and K. Kremer, *Science*, 2004, **303**, 823.
- (33) M. Rubinstein and R. H. Colby, *Polymer Physics*, Oxford Univ. Press: New York, 2003.
- (34) R. H. Colby, D. C. Boris, W. E. Krause and S. Dou, *Rheol. Acta*, 2007, **46**, 569.
- (35) E. Helfand and J. Skolnick, *J. Chem. Phys.*, 1982, **77**, 5714.
- (36) D. Auhl, J. Ramirez, A. E. Likhtman, P. Chambon and C. Fernyhough, *J. Rheol.*, 2008, **52**, 801.
- (37) C. Baig, V. G. Mavrantzas and M. Kröger, *Macromolecules*, 2010, **43**, 6886.
- (38) M. H. N. Sefiddashti, B. J. Edwards and B. Khomami, *J. Rheol.*, 2015, **59**, 119.

- (39) M. H. N. Sefiddashti, B. J. Edwards and B. Khomami, *J. Rheol.*, 2016, **60**, 1227.
- (40) C. N. Edwards, M. H. N. Sefiddashti, B. J. Edwards and B. Khomami, *J. Mol. Graph. Model.* 2018, **81**, 184.
- (41) T. C. O'Connor, N. J. Alvarez, M. O. Robbins, 2018, *arXiv:1806.09509* [cond-mat.soft].
- (42) P. E. Boukany, Y. Hu and S.-Q. Wang, *Macromolecules*, 2008, **41**, 2664.
- (43) S. Ravindranath, S.-Q. Wang, M. Olechnowicz and R. P. Quirk, *Macromolecules*, 2008, **41**, 2663.
- (44) S. Cheng and S.-Q. Wang, *J. Rheol.*, 2012, **56**, 1413.
- (45) J. Cao and A. E. Likhtman, *Phys. Rev. Lett.* 2012, **108**, 028302.
- (46) M. Mohagheghi and B. Khomami, *Phys. Rev. E*, 2016, **93**, 062606;
- (47) Y. Wang and S.-Q. Wang, *J. Rheol.*, 2008, **52**, 1275.
- (48) G. Liu, H. Sun, S. Rangou, K. Ntetsikas, A. Avgeropoulos and S.-Q. Wang, *J. Rheol.*, 2013, **57**, 89.
- (49) A. Ya. Malkin and C. J. S. Petrie, *J. Rheol.*, 1997, **41**, 1.
- (50) X. Zhu and S.-Q. Wang, *J. Rheol.*, 2013, **57**, 223.

for Table of Contents use only



Deformation-induced changes of tube confinement field significantly modifies the shear rheological response of entangled flexible polymer liquids at  $Wi_R < 1$ .